Research Article | Vol. 29, No. 15 / 19 July 2021 / Optics Express 23799
Optics EXPRESS

Passively Q-switched 914 nm microchip laser for lidar systems

MARCO NÄGELE,[1,2] KLAUS STOPPEL,[1] AND THOMAS DEKORSY[2,3,*]

[1]Robert Bosch GmbH, Cross-Domain Computing Solutions (XC), Stuttgart, Germany
[2]Institute of Aerospace Thermodynamics, University of Stuttgart, Germany
[3]Institute of Technical Physics, German Aerospace Center (DLR), Stuttgart, Germany
[*]Thomas.Dekorsy@dlr.de

Abstract: Passively Q-switched microchip lasers enable great potential for sophisticated lidar systems due to their compact overall system design, excellent beam quality, and scalable pulse energies. However, many near-infrared solid-state lasers operate at >1000 nm which are not compatible with state-of-the-art silicon detectors. Here we demonstrate a passively Q-switched microchip laser operating at 914 nm. The microchip laser consists of a 3 mm long Nd^{3+}:YVO_4 crystal as a gain medium while Cr^{4+}:YAG with an initial transmission of 98% is used as a saturable absorber. Quasi-continuous pumping enables single pulse operation and low duty cycles ensure low overall heat generation and power consumption. Thus, thermally induced instabilities are minimized and operation without active cooling is possible while ambient temperature changes are compensated by adjustment of the pump laser current only. Single-emitter diode pumping at 808 nm leads to a compact overall system design and robust setup. Utilization of a microchip cavity approach ensures single-longitudinal mode operation with spectral bandwidths in the picometer regime and results in short laser pulses with pulse durations below 10 ns. Furthermore, beam quality measurements show that the laser beam is nearly diffraction-limited. A 7% output coupler transmittivity is used to generate pulses with energies in the microjoule regime and peak powers of more than 600 W. Long-term pulse duration, pulse energy, and spectral wavelength measurements emphasize excellent system stability and facilitate the utilization of this laser in the context of a lidar system.

1. Introduction

Nowadays, light detection and ranging (lidar) systems are indispensable. For example, in metrology, weather and climate [1–3] data are collected using lidar systems, while in agriculture, deforestation [4], terrain profiles [5], and the targeted distribution of fertilizers [6] can be mapped. Likewise, lidar sensors can be used for object detection and thus are taking on an important role in the mobility of the future, where these systems are considered as one of the key technologies for automated driving [7]. For lidar systems the application possibilities are as numerous as the demands to the sensor, with the laser contributing significantly to the overall performance of the system in general.

In addition to the commonly used pulsed semiconductor lasers, passively Q-switched solid-state lasers in particular offer huge potential. These lasers usually have diffraction-limited beam quality, scalable pulse energies up to double-digit mJ [8,9], and feature simple driver circuits without high peak currents, which in turn reduces EMC susceptibility. Moreover, for microchip laser cavities short pulse durations in the single-digit nanosecond range, as well as operation on only one longitudinal mode is possible [10]. Combined with the small temperature-dependent wavelength shift [11], narrowband filters can be utilized to significantly improve the signal-to-noise ratio at the detector.

#432340 https://doi.org/10.1364/OE.432340
Journal © 2021 Received 27 May 2021; revised 24 Jun 2021; accepted 25 Jun 2021; published 12 Jul 2021

Optics EXPRESS

While in semiconductor lasers the emitting wavelength can be shifted by design, solid-state lasers have fixed atomic transitions and are thus much more limited. These solid-state laser transitions are often located in the near- and far-infrared spectral range above one micrometer. It is therefore not surprising that the best known solid-state laser based on Nd^{3+}:YAG has its strongest emission wavelength at 1064 nm, and that a lot of investigations have already been carried out here, both in pulsed and continuous-wave operation. In contrast, there are comparatively few laser crystals that can be operated at emission wavelengths in the near-infrared spectrum (NIR) below 1000 nm. Primarily, various Nd^{3+}-doped host materials such as Nd^{3+}:YAG at 946 nm [12], Nd^{3+}:YVO_4 at 914 nm [13], or Nd^{3+}:$GdVO_4$ at 912 nm [14] can be considered here.

However, for future lidar systems, these lasers in pulsed operation mode are necessary to enable the use of comparatively inexpensive state-of-the-art silicon detector technology, which has been well established so far and is widely available on the market. The problem for the missing pulsed lasers in the NIR below 1 µm is apparent. To achieve a narrow band spectral transition, only rare-earth active ions come into account and here only Nd^{3+}- ions in combination with certain host crystals have the desired spectral transition below one micron in the form of a quasi-three-level laser. Especially these quasi-three-level lasers are more difficult to implement compared to the classical four-level systems above one micron. First, for these quasi three-level lasers, the stimulated-emission cross-section is about one order of magnitude smaller, which is the reason why high resonator losses for the undesired four-level transition have to be generated by the cavity coatings. Apart from that, the coating-induced reflectivity for the desired emission wavelength has to be as high as possible, while on the pump facet a high transmission of the pump wavelength has to be ensured. This sets high demands on the optical coating to operate the laser on the desired wavelength as loss-free as possible and thus with maximum efficiency. A second limitation for quasi-three-level systems is reabsorption since the lower laser level also forms the upper ground-state manifold and therefore has a non-negligible thermal occupancy. In general, the application of these lasers requires a compact and robust, if possible monolithic, cavity design without active temperature control.

So far only few passively Q-switched quasi-three-level microchip lasers based on Nd^{3+}:YAG have already been successfully investigated [15–17], whereas Nd^{3+}:YAG has several disadvantages compared to Nd^{3+}:YVO_4.

For instance, the stimulated-emission cross-section but also the absorption cross-section is smaller [18,19], the isotropy of the YAG host crystal leads to random linear polarization with additional depolarization losses [20], and the wavelength of the quasi-three-level transition leads to poorer quantum efficiency in commercially available silicon detectors [21]. Through this, various systems at 914 nm have been demonstrated in the past in CW [13], passively Q-switched [22,23], and mode-locked [24,25] operation. Compared to previous research, in this work, we investigated a passively Q-switched Nd^{3+}:YVO_4 microchip laser at 914 nm and demonstrated the enormous potential in terms of lidar applications.

2. Experimental setup

The setup of the passive Q-switched microchip laser is shown in Fig. 1. A single emitter pump diode with a central wavelength of 808 nm and a maximum output power of 15 W was used (Sheaumann CL-808-015W-430). Initially, the pump laser was thermally coupled to a cooling water circuit, through which the laser temperature and consequently the central wavelength could be adjusted. Compared to a fiber-coupled pump laser, the single emitter pump laser is much more compact, cheaper, and has a narrower spectral bandwidth. Two cylindrical lenses with focal lengths of 15 mm and 35 mm were used to focus the rectangular pump laser aperture onto a square pump spot of approximately 220 µm ($\sim 1/e^2$). Using a half-wave plate, the preferred direction of pump polarization could be adjusted to optimize the system during subsequent laser operation. The microchip resonator consisted of a 3 mm long and 0.15% at doped Nd^{3+}:YVO_4

Optics EXPRESS

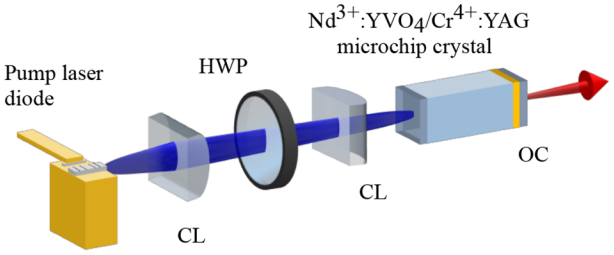

Fig. 1. Experimental setup of the passively Q-switched Nd^{3+}:YVO_4/Cr^{4+}:YAG microchip laser. CL: cylindrical lens, HWP: half-wave plate, OC: output coupler.

crystal (a-cut, Casix Inc.) which was bonded to a Cr^{4+}:YAG saturable absorber with an initial transmission of 98%. For the length and doping of the gain medium, a trade-off was made between absorption of the pump light, reabsorption of the laser light and pulse duration. Basically, the gain medium should be selected with a length and doping concentration such that the incident pump power is completely absorbed. On one hand, by choosing a longer gain crystal the complete pump power is absorbed but the non-pumped end of the crystal leads to reabsorption of the laser light while comparatively little pump light is absorbed. Also, a longer gain medium extends the resonator length and thus increases the pulse duration, which is proportional to the resonator round-trip time of the photons. If, on the other hand, the doping concentration is increased, the reabsorption also increases, and in the case of too high doping, quenching effects occur that reduce the fluorescence lifetime and consequently the pulse energy. According to Lambert's law, for the selected gain crystal length of 3 mm and doping concentration of 0.15% at about 93% of the pump power is absorbed in the crystal, while the pulse duration remains quite short and the reabsorption comparatively small.

The microchip crystal was wrapped with indium foil and mounted in a copper holder. The dielectric coupling coating was transparent to pump light and highly reflective for 914 nm while the decoupling mirror had a transmittivity of 7% at the laser wavelength. To suppress parasitic laser oscillations, the dielectric resonator mirrors were specified with an anti-reflective coating (R<0.5%) at 1064 nm and 1342 nm.

According to the literature, the value for the stimulated-emission cross-section of the $^4F_{3/2} \rightarrow {}^4I_{9/2}$ transition was determined to be 4.8×10^{-20} cm^2 [18] while an upper laser level lifetime of 100 µs at 293 K [26] was determined. Furthermore, a thermal fractional population of 0.406 and 0.048 was calculated at room temperature (293 K) for the lower and upper Stark splittings of the ground state ($^4I_{9/2}$), respectively. The upper splitting is simultaneously the lower laser level in the quasi-three-level system.

3. Experimental investigations

To demonstrate the potential for lidar systems, the passive Q-switched microchip laser was operated at a repetition rate of 200 Hz and investigated for stability properties that are important for various applications in the lidar context. Hereby, the repetition rate of 200 Hz was not the upper stability limit of the system in terms of repetition rate, but a deliberately chosen parameter since further measurements are planned in a proof-of-principle lidar application.

3.1. Pumping scheme

While passively Q-switched solid-state lasers usually have repetition rates in the kilohertz range during continuous pumping, a quasi-continuous (QCW) pumping scheme was used in this work to set a pulse repetition rate of 200 Hz with the single-pulse operation. Figure 2 shows the time evolution of the pump current applied by the laser driver (Ostech ds11-la14v14) in blue,

Optics EXPRESS

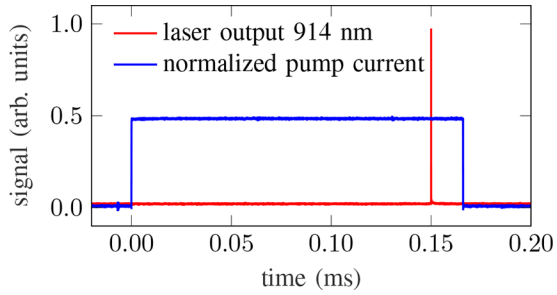

Fig. 2. Quasi-continuous pumping scheme for generating single laser pulses with a repetition rate of 200 Hz and a low duty cycle of about 3.4%. The current applied to the pump laser is displayed in blue, while the pulsed laser output is shown in red.

while pumping was performed for a time duration of 170 µs. Shown in red is the generated laser signal at 914 nm which was separated from the remaining pump signal behind the microchip laser by a bandpass interference filter (Edmund Optics 900 nm x 25 nm) and recorded with a fast InGaAs detector (5 GHz bandwidth, Thorlabs) in combination with a 6 GHz oscilloscope (LeCroy WavePro 804HD). QCW pumping with a period of 5 ms (200 Hz) resulted in a low duty cycle of only 3.4% which minimized the thermal load in the crystal and prevented the need for active cooling of the monolithic crystal. The amplitude of the current was chosen such that the laser pulse was generated with respect to the rising current edge after a delay time of 150 µs. The required current amplitude to generate a laser pulse with a delay time of 150 µs is strongly dependent on the pump laser temperature. Since the pump laser in use is an edge emitter, a temperature-dependent wavelength shift of 0.3 nm K^{-1} is expected while the output power and efficiency additionally decrease for increasing temperatures [27]. Consequently, a change in ambient temperature has a large impact on the overall solid-state laser performance if the pump laser is not actively temperature stabilized. Since in this work an active temperature control was not intended, it was investigated to what extent the temperature influence of the pump laser could be compensated by a current adjustment to keep the generated laser pulse at a constant delay of 150 µs.

Figure 3 shows the experimental investigations in this context. Here, the current required at the pump laser is plotted against the temperature of the pump laser. In this measurement, the

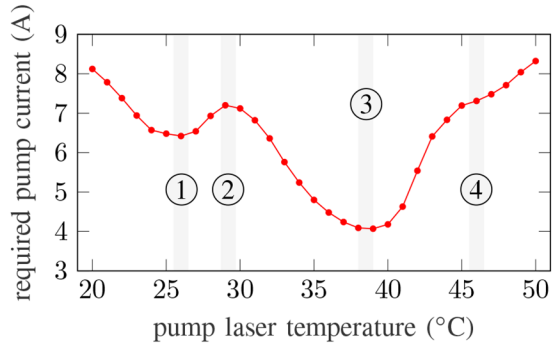

Fig. 3. Required pump laser current as a function of pump laser temperature to generate laser pulses with a constant delay of 150 µs concerning the switch-on of the pump laser. The numbers 1 to 4 mark distinctive positions at which different effects dominate in the interaction between the pump laser and the properties of the laser crystal.

Optics EXPRESS

pump laser was temperature-controlled in one degree Celsius steps using a cooling water circuit to temperatures between 20 °C and 50 °C. Subsequently, the pump current at the laser driver was adjusted to maintain a constant pulse delay of 150 µs from the rising pump edge to the generated laser pulse. The numbers from ① to ④ mark distinctive points at which different effects in the interaction between pump laser and the properties of the laser crystal dominate. The shape of the measured curve results from the superposition of the intrinsic Nd^{3+}:YVO_4 absorption spectrum and the temperature dependence of the pump laser in terms of wavelength and output power. In the following discussion features in the absorption spectrum of Nd^{3+}:YVO_4 are mentioned which have been studied by McDonagh and Wallenstein in detail for c-cut and a-cut crystals [28]. The lowest pumping current and thus the global minimum was reached in our experiment for a pumping temperature of 39 °C and is marked by position ③. This minimum results from the good spectral overlap between the narrow-band pump lasers with the maximum absorption peak of Nd^{3+}:YVO_4 at 808 nm. Starting from this point, if the cooling water temperature was reduced, the applied pump power increased slightly but the overlap between the narrow-band absorption peak and the single emitter became worse. Consequently, the required pumping current increased. At position ②, the pump power was greater than at point ③ for the identical current, but due to the blue shift of the pump wavelength, a larger current was required for delay compensation of the laser pulse. With decreasing temperature, a local minimum of 6.42 A was again reached in ① at 26 °C. This was a result due to a side-wing peak of the absorption spectrum in combination with the increasing output power of the pump laser for lower temperatures. A further lowering of the temperature finally led to a significant reduction of the spectral overlap, which could no longer be compensated by the slightly increasing pump power due to a lower temperature. From the global minimum in ③, a larger pump laser current was also required with increasing temperature to maintain the laser pulse at a constant level due to spectral shifting. In region ④, a slight correction of the rising current slope could be observed, which probably also arised from a lateral absorption peak next to the main maximum at 808 nm (see the spectrum at [28]). For increasing temperatures, the semiconductor laser spectrum shifted to a larger wavelength and the overlap with the absorption band of Nd^{3+}:YVO_4 deteriorated. Additionally, the output power of the pump laser decreased for increasing temperatures while no adaptation of the electric current was made.

In addition to the temperature effects of the pump laser, another experiment was conducted to investigate the temperature effects of the microchip laser crystal on the pulse delay time. By adjusting the cooling water temperature of the crystal holder in the range of 20 °C to 50 °C, only a small influence on the delay time of the solid-state laser pulse was observed. This effect could be compensated easily by a slight adjustment of the pump laser current in the range of several 0.05 A.

In total the experiment revealed that the overall laser system can be operated stably without active temperature control in the range 20-50 °C simply by adjustment of the pump laser current.

3.2. Output characteristics

In the following, the output parameters such as pulse duration, spectral width, and beam quality are examined. Moreover, the stability of the pulse energy, pulse duration, and the resulting peak power, as well as the stability of the wavelength were measured.

All subsequent measurements were performed with a pump laser current of 7.91 A, which corresponded to an average pump power of 269 mW. With the applied duty cycle of 3.4% (179 µs/200 µs), this resulted in a peak pump power of 7.9 W.

For lidar sensors, the pulse duration is an important parameter, since it has a considerable influence on the longitudinal resolution of the system. For that reason, an estimate of the pulse duration is performed in the beginning. In the case of passively Q-switched lasers, the exponentially growing photon field typically requires several resonator cycles until the majority

Optics EXPRESS

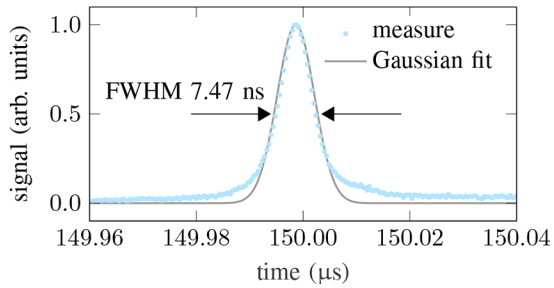

Fig. 4. Oscilloscope trace of a laser pulse (light blue) with a pulse duration of 7.47 ns (FWHM). The pulse duration was determined by a fit (gray) assuming a Gaussian pulse shape.

of the stored energy in the gain medium is extracted. As a rough estimate, in the case of passive Q-switching with strong saturation the pulse duration τ_p can be estimated by

$$\tau_p \approx 4.60 \, \frac{T_\mathrm{r}}{q_0}. \tag{1}$$

Here, T_r is the photon resonator round trip time and q_0 ~ (1 - $\mathrm{T_0}$) are the saturable losses considering an initial transmission $\mathrm{T_0}$ and no non-saturable losses of the saturable absorber. For the microchip laser used here, we obtain an estimated pulse duration of 9.64 ns, taking into account the refractive index of Nd^{3+}:YVO_4 and the initial transmission of 98%. It was expected that a short pulse duration is possible due to the short resonator length of the microchip laser and thus the short signal round-trip time. Likewise, lower initial transmissions lead to a larger population inversion in the laser crystal and thus to a faster buildup of the electric field in the cavity.

The experimental measurement of the pulse duration is shown in Fig. 4 and is an enlargement of the pump scheme from Fig. 2 around the range of the generated laser pulse. Assuming a

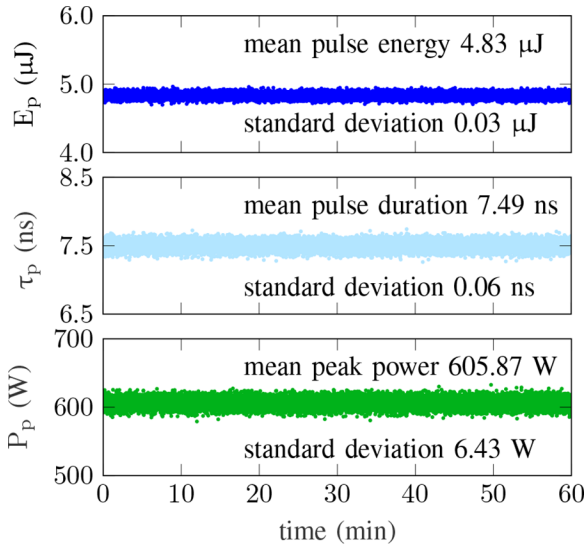

Fig. 5. Pulse energy (top), pulse duration (middle), and the calculated peak power (bottom) recorded over 60 minutes.

Optics EXPRESS

Gaussian pulse shape, fitting results in a pulse duration of 7.47 ns (FWHM) which is in reasonable agreement with the estimated value of 9.64 ns.

The long-term stability of pulse energy, pulse duration and the resulting peak power is shown in Fig. 5 and was measured simultaneously 60 minutes. For this purpose, both the pump laser and the microchip crystal were disconnected from the cooling water supply and the system was operated at room temperature (20.5 °C according to the laboratory thermometer). The laser was warmed up for 10 minutes to reach thermal equilibrium before the measurement was started. For the stability measurement, a pump current of 7.91 A was required at the laser driver, in agreement with Fig. 3, to generate laser pulses with a delay time of 150 µs. A pyroelectric energy sensor (Ophir PE9-C) was used to measure the pulse energy. In the upper part of Fig. 5, the measurement of the pulse energy is depicted in dark blue. Over 60 minutes, an average pulse energy of 4.83 µJ was determined with a standard deviation of 0.03 µJ. This corresponds to a fluctuation of just 0.62% which is a remarkable value considering the absence of an active temperature control [29]. The obtained pulse energy was comparatively small but for future experiments, it should in principle be possible to increase this significantly. For this purpose, on one hand, the pump spot can be enlarged, thus increasing the effective area on the saturable absorber. On the other hand, a smaller value for the initial transmission of the saturable absorber and a larger decoupling transmissivity could be chosen. In this way, pulse energies in the 10-100 mJ regime have already been generated for other passively Q-switched lasers [8,9,30].

The stability measurement of the pulse duration is shown in light blue in the center of Fig. 5 and was recorded analogously to Fig. 4 using the fast InGaAs detector with a bandwidth of 5 GHz. A mean pulse duration of 7.49 ns and a standard deviation of 0.06 ns ($\widehat{=}$ 0.80%) were measured for one hour.

Further, for a given pulse energy and pulse duration the peak power can be determined assuming a Gaussian pulse shape, by using [31]

$$P_p \approx 0.94 \, \frac{E_p}{T_p}. \tag{2}$$

Here, E_p is the pulse energy, T_p is the pulse duration and 0.94 is a correction factor taking into account a Gaussian pulse shape. Since the pulse energy and pulse duration were measured simultaneously, Eq. (2) can be used to calculate the corresponding peak power, which is shown in green in the lower part of Fig. 5. The mean calculated peak power is 605.87 W, which corresponds to a peak power stability with a standard deviation of 6.43 W linked to 1.06%. Next, the spectral properties were investigated. In general, if the resonator of solid-state lasers with a narrow bandwidth gain medium is kept very short, they can operate on a single longitudinal mode with a spectral width of only a few picometers [10,32]. Additionally, passive Q-switching, compared to CW operation, causes the laser to further reduce the number of modes. In theory, the mode that bleaches the saturable absorber has some advantage in terms of photon number over competing longitudinal modes in the race for the laser gain. Thus, this single-mode already reduces almost the complete population inversion in the gain crystal by its exponential growth, while other modes are additionally suppressed by the missing gain [33,34].

For applications, the combination of a single longitudinal mode along with the small temperature-dependent wavelength shift of solid-state lasers (a few picometers per degree Kelvin [11]) allows the use of extremely narrowband spectral filters and thus an excellent signal-to-noise ratio at the detector.

In this work, the spectrum of the passively Q-switched microchip laser was recorded with a high-resolution hyperfine spectrometer (Lightmachinery HF-8991-3, 2.0 pm minimum resolution according to manufacturer). The resulting spectrum is shown in Fig. 6 and indicates that the laser operates in a single longitudinal mode. The calculated central wavelength of this mode was 913.986 nm, while a spectral width (FWHM) of 3.3 pm was observed.

Optics EXPRESS

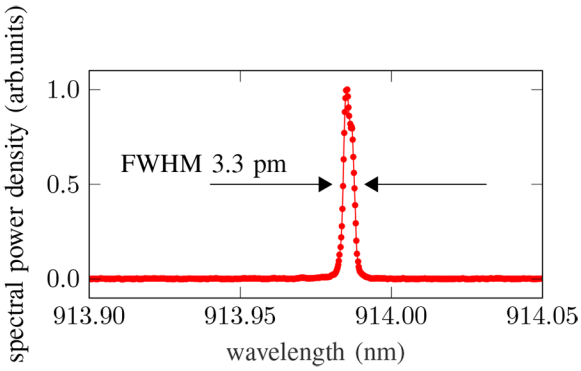

Fig. 6. Spectrum of a single longitudinal mode with a spectral bandwidth of 3.3 pm (FWHM) at a center wavelength of approximately 914 nm.

Similar to the previous stability study of the pulse energy, pulse duration, and peak power, the spectral stability of the longitudinal mode was investigated for 60 minutes. Figure 7 shows the temporal stability of the spectrum, where individual spectra were recorded at a sampling rate of 1 sample/second and then lined up to an intensity map in a post-processing process using MATLAB. In the graph, small fluctuations which are possibly due to the lack of annealing can be seen, yet the spectrum remains extremely stable and no other competing longitudinal mode could be observed. Post-processing of the individual spectra was performed with a Gaussian fit and yielded a standard deviation of 4.2% around the central wavelength of 913.986 nm. For the spectral bandwidth, the analysis results in a mean value of 3.4 pm with a standard deviation of 4.96%. Finally, for the beam quality measurements, the pulsed laser light was coupled into a beam propagation analyzer (Ophir BSQ-SP920) after the bandpass filter which blocked the residual pump light. Beam analysis was performed using a 400 mm lens in triggered operation mode to determine the beam quality, divergence angle, and back-calculated resonator foci.

Figure 8 shows the measured beam radius in the x- and y-axis as a function of propagation position. The inset is taken at a position of 900 mm and shows the transverse beam profile with a nearly Gaussian intensity distribution. In both directions, the beam was nearly diffraction-limited with an M^2 of 1.18 and 1.14 and a full divergence angle of 2.03 mrad and 1.64 mrad in the x- and y-directions, respectively. The back-calculated waist diameters at the foci of the laser were 168.8 µm and 202.6 µm (x- and y-direction), which is almost a factor of 1.7 smaller than the predefined pump spot radius of about 100 µm. Using this information, in future experiments the

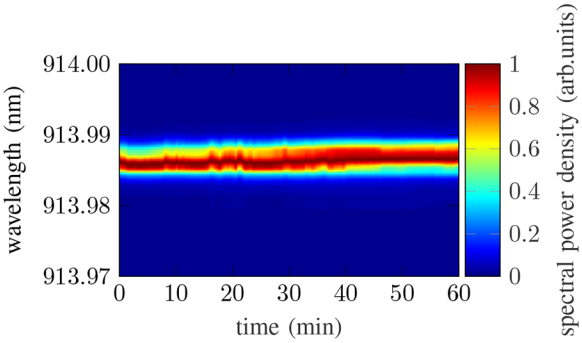

Fig. 7. Stability measurement of the laser spectrum recorded over 60 min at a sampling rate of 1 Hz without active cooling of the pump laser and the monolithic crystal.

Optics EXPRESS

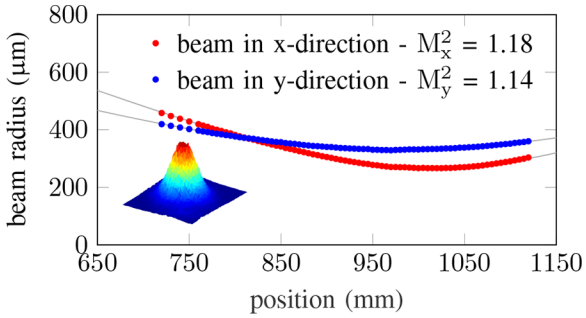

Fig. 8. Beam quality measurement with associated beam radii in x- and y-direction as a function of position z. The inset shows the transverse near Gaussian beam profile at a position of 900 mm.

pump optics can be adjusted and optimized, presumably reducing the asymmetry between the two beam directions. For lidar applications, the excellent near Gaussian beam quality can be used to obtain high-resolution images as the beam could be focused to almost the minimum spot size in both respective directions.

For future investigations, the edge emitter pump laser diode could be replaced by a surface-emitting semiconductor laser array with a quadratic pattern. This would have the advantage that a single pump lens could be used instead of the two cylindrical lenses to image the pump light squarely in the laser crystal. Furthermore, the smaller temperature-dependent pump wavelength shift of the surface emitter (0.06 nm/K vs. 0.3 nm/K) would lead to a larger operating range while matching the ambient temperature (see Fig. 3). Also, it would be conceivable to use a wavelength-stabilized laser diode. In addition to this, it would be interesting to record the average output power as a function of input power at different temperatures to get a better and more detailed system understanding concerning pulse energy scalability and pulse build-up time. Moreover, the temporal jitter between the individual pulses could be recorded and analyzed as a function of the pump power.

4. Conclusion

We demonstrated a passively Q-switched microchip laser based on Nd^{3+}:YVO_4 and Cr^{4+}:YAG and showed its potential for lidar system applications. By quasi-continuous pumping at a frequency of 200 Hz, the thermal load in the crystal was minimized and no active cooling was required to operate the system. Furthermore, it was shown that the whole microchip laser can be operated without cooling in a temperature range between 20-50 °C by adjusting the pump current only. The short monolithic resonator produced short pulse durations well below 10 ns and operation on a single longitudinal mode with a spectral width of only a few picometers was possible. The quasi-three-level operation of the system allowed an emission wavelength of 914 nm ensuring compatibility with state-of-the-art silicon detectors. Further, beam quality studies showed that the laser is nearly diffraction-limited with an M^2 better than 1.2 in both directions. Stability measurements of pulse energy, pulse duration, peak power, and wavelength underline the great potential of this system. The passively Q-switched microchip laser shown here served as a kind of proof-of-principle for the underlying potential and formed the basis for future investigations and possible optimizations. Thus, by adjusting the initial transmission, the pump spot, and the outcoupling reflectivity, it should be possible to generate significantly larger pulse energies in any case, while the repetition rate offers a wide range of applications by QCW pumping.

Optics EXPRESS

Disclosures. The authors declare no conflicts of interest.

Data availability. Data underlying the results presented in this paper are not publicly available at this time but may be obtained from the authors upon reasonable request.

References

1. J. Bilbro, G. Fichtl, D. Fitzjarrald, M. Krause, and R. Lee, "Airborne doppler LiDAR wind field measurements," Bull. Am. Meteorol. Soc. **65**(4), 348–359 (1984).
2. R. T. Menzies and R. Michael Hardesty, "Coherent doppler LiDAR for measurements of wind fields," Proc. IEEE **77**(3), 449–462 (1989).
3. M. Wirth, A. Fix, P. Mahnke, H. Schwarzer, F. Schrandt, and G. Ehret, "The airborne multi-wavelength water vapor differential absorption LiDAR WALES: System design and performance," Appl. Phys. B: Lasers Opt. **96**(1), 201–213 (2009).
4. K. Lim, P. Treitz, M. Wulder, B. St-Ongé, and M. Flood, "LiDAR remote sensing of forest structure," Prog. Phys. Geogr. **27**(1), 88–106 (2003).
5. J. A. Bellian, C. Kerans, and D. C. Jennette, "Digital outcrop models: Applications of terrestrial scanning LiDAR technology in stratigraphic modeling," J. Sediment. Res. **75**(2), 166–176 (2005).
6. K. Koenig, B. Höfle, M. Hämmerle, T. Jarmer, B. Siegmann, and H. Lilienthal, "Comparative classification analysis of post-harvest growth detection from terrestrial LiDAR point clouds in precision agriculture," ISPRS J. Photogramm. Remote Sens. **104**, 112–125 (2015).
7. J. Hälker and H. Barth, "LiDAR as a key technology for automated and autonomous driving," ATZ Worldw. **120**(S1), 70–73 (2018).
8. A. Kausas and T. Taira, "Giant-pulse Nd:YVO_4 microchip laser with MW-level peak power by emission cross-sectional control," Opt. Express **24**(4), 3137 (2016).
9. A. Maleki, M. H. Moghtader dindarlu, H. Saghafifar, M. Kavosh Tehrani, M. Soltanolkotabi, M. Dehghan Baghi, and M. R. Maleki Ardestani, "57 mJ with 10 ns passively Q-switched diode pumped Nd:YAG laser using Cr^{4+}:YAG crystal," Opt. Quantum Electron. **48**(1), 48 (2016).
10. T. Taira, A. Mukai, Y. Nozawa, and T. Kobayashi, "Single-mode oscillations of laser-diode-pumped Nd:YVO_4," (1991).
11. Y. Sato and T. Taira, "Temperature dependencies of stimulated emission cross section for Nd-doped solid-state laser materials," Opt. Mater. Express **2**(8), 1076 (2012).
12. R. Zhou, T. Zhang, E. Li, X. Ding, Z. Cai, B. Zhang, W. Wen, P. Wang, and J. Yao, "8.3 W diode-end-pumped continuous-wave Nd:YAG laser operating at 946-nm," Opt. Express **13**(25), 10115–10119 (2005).
13. P. Jiang, "Efficient 914-nm Nd:YVO_4 laser under double-end polarized pumping," Appl. Opt. **55**(5), 1072–1075 (2016).
14. J. Gao, X. Yu, F. Chen, X. Li, R. Yan, K. Zhang, J. Yu, and Y. Wang, "120-W continuous-wave diode-end-pumped Nd:$GdVO_4$ laser with high brightness operating at 912-nm," Opt. Express **17**(5), 3574 (2009).
15. L. Lv, L. Wang, P. Fu, X. Chen, Z. Zhang, V. Gaebler, D. Li, B. Liu, and H. J. Eichler, "Diode-pumped self-Q-switched single-frequency 946-nm Nd^{3+}, Cr^{4+}:YAG microchip laser," Opt. Lett. **26**(2), 72–74 (2001).
16. X. B. Chen, L. Wang, L. B. Lv, Z. G. Zhang, J. G. Zhu, W. M. Du, G. Z. Yang, G. W. Wang, and G. Kyle, "Study of 946 nm microchip self-Q-switched monofrequency laser," Opt. Commun. **224**(4-6), 275–280 (2003).
17. B. M. Walsh, "Tunability of a 946-nm Nd:YAG microchip laser versus output mirror reflectivity and crystal length," Opt. Eng. **43**(12), 3026 (2004).
18. F. Chen, J. Sun, R. Yan, and X. Yu, "Reabsorption cross section of Nd^{3+} -doped quasi-three-level lasers," (2019).
19. P. S. Ebrahim, B. Noriah, and B. Hazri, "Temperature and input energy dependence of the 946-nm stimulated emission cross section of Nd^{3+}:YAG pumped by a flashlamp," Lett. Chinese Phys. **29**(3), 034206 (2012).
20. H. J. Eichler, A. Haase, R. Menzel, and A. Siemoneit, "Thermal lensing and depolarization in a highly pumped Nd:YAG laser amplifier," J. Phys. D: Appl. Phys. **26**(11), 1884–1891 (1993).
21. U. Kindereit, A. J. Weger, and P. Song, "Near-Infrared Photon Emission Spectroscopy of a 45 nm SOI Ring Oscillator," in *Proceedings of IEEE Conference on Reliability Physics Symposium* (IEEE, 2012).
22. X. Yu, R. Yan, X. Li, Y. Ma, D. Chen, and Y. Junhua, "High power 2 MHz passively Q-switched nanosecond Nd:YVO_4/Cr^{4+}:YAG 914 nm laser," Appl. Opt. **51**(14), 2728–2732 (2012).
23. M. Nägele, K. Stoppel, H. Ridderbusch, and D. Thomas, "Passively Q-switched Nd:YVO_4 laser operating at 914 nm," in *Proceedings of SPIE Conference on LASE* (SPIE, 2020).
24. A. Schlatter, L. Krainer, M. Golling, and R. Paschotta, "Passively mode-locked 914-nm Nd:YVO_4 laser," Opt. Lett. **30**(1), 44–46 (2005).
25. P. Blandin, F. Druon, F. Balembois, P. Georges, S. Lévêque-Fort, and M. P. Fontaine-Aupart, "Diode-pumped passively mode-locked Nd:YVO_4 laser at 914 nm," Opt. Lett. **31**(2), 214 (2006).
26. J. G. Sliney, K. M. Leung, M. Birnbaum, and A. W. Tucker, "Lifetimes of the $^4F_3/2$ state in Nd:YVO_4," J. Appl. Phys. **50**(5), 3778–3779 (1979).
27. N. I. Khan, S. H. Choudhury, and A. A. Roni, "A comparative study of the temperature dependence of lasing wavelength of conventional edge emitting stripe laser and vertical cavity surface emitting laser," in *Proceedings of IEEE Conference on Optical Communication Systems* pp. 141–145 (IEEE, 2011).

Optics EXPRESS

28. L. McDonagh, R. Wallenstein, R. Knappe, and A. Nebel, "High-efficiency 60 W TEM_{00} Nd:YVO_4 oscillator pumped at 888 nm," Opt. Lett. **31**(22), 3297 (2006).
29. R. S. Cudney and C. Minor, "Sub-nanosecond, megawatt compact diode-pumped Nd:YLF laser," Rev. Mex. Física **64**(5 Sept-Oct), 512–518 (2018).
30. M. Tsunekane, T. Inohara, A. Ando, N. Kido, K. Kanehara, and T. Taira, "High peak power, passively Q-switched microlaser for ignition of engines," IEEE J. Quantum Electron. **46**(2), 277–284 (2010).
31. R. Paschotta, *Field Guide to laser pulse generation* (SPIE Book, 2008).
32. H. Sakai, H. Kan, and T. Taira, ">1 MW peak power single-mode high-brightness passively Q-switched Nd^{3+}:YAG microchip laser," Opt. Express **16**(24), 19891–19899 (2008).
33. D. Jin, Z. Bai, Q. Wang, Y. Chen, Z. Liu, R. Fan, Y. Qi, J. Ding, X. Yang, Y. Wang, and Z. Lu, "Doubly Q-switched single longitudinal mode Nd:YAG laser with electro-optical modulator and Cr:YAG," Opt. Commun. **463**, 125500 (2020).
34. W. R. Sooy, "The natural selection of modes in a passive Q-switched laser," Appl. Phys. Lett. **7**(2), 36–37 (1965).